Observations of the vacuum ultraviolet and x-ray brightness profiles of Fe, Ni, and Ge in magnetically confined fusion plasmas

M. J. May,* M. Finkenthal, and H. W. Moos
Plasma Spectroscopy Group, Department of Physics and Astronomy, The Johns Hopkins University, 34th and North Charles Streets, Baltimore, Maryland 21218

K. B. Fournier and W. H. Goldstein
Lawrence Livermore National Laboratories, P.O. Box 808 L41, Livermore, California 94551

M. Mattioli, D. Pacella, G. Mazzitelli, M. Leigheb, and L. Gabellieri
FTU, Associazione EURATOM ENEA sulla Fusione, Frascati (Roma) 00044, Italy
(Received 9 March 2001; published 30 August 2001)

The spatial brightness profiles of emission lines for the K-like through He-like ionization states of Fe, Ge, and Ni have been measured during a set of experiments in which Fe and Ge were introduced into FTU tokamak plasmas by using the laser blowoff technique. Nickel was an intrinsic impurity observed during these experiments that was sputtered from the inconel limiter. The brightness profiles were measured by spatially scanable, photometrically calibrated vaccum ultraviolet and x-ray spectrometers that covered the 1 to 1700 Å region. Simulations of these profiles and the time evolution of the laser blowoffs were performed with the MIST transport code using several sets of atomic physics compilations [ADPAK (originally in MIST), Arnaud and Raymond (AR92), Arnaud and Rothenflug (AR85), Mazzotta *et al.*, and Mattioli (an extension to Mazzotta)]. The goal was to determine which set of available rates could best simulate the measured spatial brightness profiles and the charge state balance in the plasma. The Mazzotta *et al.* (for Fe and Ni), the Mattioli (for Ge), and the AR92 (for Fe only) rates adequately simulated the He-, Li-, Be-, Na-, Mg-like ionization states. The F- to B-like charge states could not be simulated by these compilations unless the relevant dielectronic rates were multiplied by a factor of 2. The ADPAK rates could not adequately predict any of the charge states of Fe, Ge, or Ni.

DOI: 10.1103/PhysRevE.64.036406 PACS number(s): 52.55.Fa, 52.25.Fi, 52.65.−y

I. INTRODUCTION

The correct prediction of the charge state distribution (CSD) of an element in a high-temperature plasma is important for many scientific investigations including magnetically confined fusion (MCF) experiments and x-ray astrophysical observations. Improvements in both the experiments (higher spectral resolution for astrophysical observations) and modeling capabilities (faster and bigger computers) have necessitated a reinvestigation of the relevant atomic physics used in the determination of the CSD.

A new age of astronomy began with the launch of the Hubble space telescope in 1990 which changed visible astronomy forever. This has been extended to the x-ray extreme ultraviolet (XUV) and x-ray with the launch of the Chanrdra x-ray observatory, the X-ray Multi-Mirror Mission (XMM), and the Far Ultraviolet Spectroscopic Explorer (FUSE). Now, astrophysics can measure the x-ray emission from celestial objects with unprecedented clarity and resolution. These satellites deduce the characteristics of astrophysical plasmas from precise spectroscopy and the ratios of different emission features of highly ionized charge states. To properly interpret the emission, sophisticated models are necessary that are based upon correct atomic physics rates (both ionization/recombination and excitation/photodecay). Compilations of ionization and recombination rates have been published by Mazzotta *et al.* [1], Arnaud and Rothenflug [2], and Arnaud and Raymond [3]. The experimental check of the resulting ionization equilibrium CSD's is necessary for proper predictions to be made.

A reexamination has also been done in recent years by our group [4–9] of the atomic physics rates used to predict the CSD of mid- to high-Z elements in magnetically confined fusion plasmas. We have applied the Hebrew University Lawrence Livermore Atomic Code (HULLAC) [10–12] to generate the ionization/recombination and excitation/photodecay rates. In these works, the inclusion of the excitation-autoionization (EA) rates in the total ionization rate was necessary to simulate properly the experimentally measured spatial brightness profiles of the impurities in the MCF plasmas. The older physics rates which were based on the average ion model of ADPAK [13] and which neglected EA were found to be inadequate.

In recent years improvements in MCF plasmas have made higher electron temperatures greater than 8 keV possible [14]. These higher temperatures are excellent for studying the atomic physics of elements with Z greater than 28 (i.e., Ge, Mo, W, and Au). A need exists for both a spectroscopic temperature measurement and a diagnostic tool for the different plasma conditions present in these higher temperature plasmas. In the reverse shear electron cyclotron resonant frequency heated (ECRH) plasmas of FTU, significant differ-

*Present address: P.O. Box 808 L260, Lawrence Livermore National Laboratories, Livermore, CA 94551.

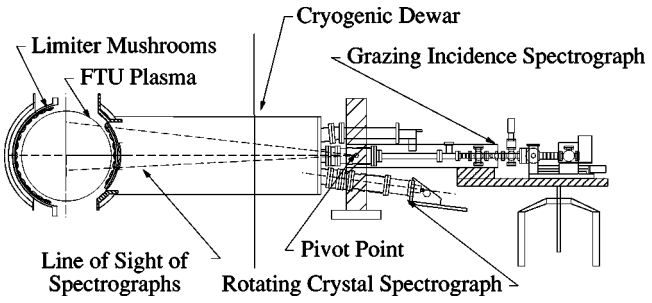

FIG. 1. Side profile of FTU Tokamak showing the spectrometers and their views of the plasma.

ences have been found in the particle transport from that observed in ohmically heated plasmas [15]. Germanium is a possible candidate for studying these effects. Therefore, in support of this work an investigation of the atomic physics and the CSD of Ge in ohmically and ECRH heated plasmas has been undertaken in FTU.

The present work concentrates on the evaluation of rates used to predict the CSD for Fe, Ge, and Ni. Iron and nickel are astrophysically relevant as well as being important for MCF plasmas. Germanium as stated above is relevant for MCF plasmas. To test the ionization/recombination atomic physics rates used to determine the CSD, the spatial brightness profiles of selected emission lines from the K-like to He-like ionization states of Fe, Ge, and Ni have been measured in the FTU Tokamak. Fe and Ge have been introduced into FTU plasmas using the laser blow off (LBO) technique [16]. Ni is an intrinsic impurity that is sputtered from the inconel limiter. The Multiple Ionization State Transport (MIST) code [17] simulated the spatial brightness profiles of the emission lines with the different compilations of ionization/recombination rates. The available compilations were those of ADPAK [13], Arnaud and Rothenflug [2], Arnaud and Raymond [3], Mazzotta *et al.* [1], and Mattioli [18]. Since the work of Mazzotta *et al.* included only H

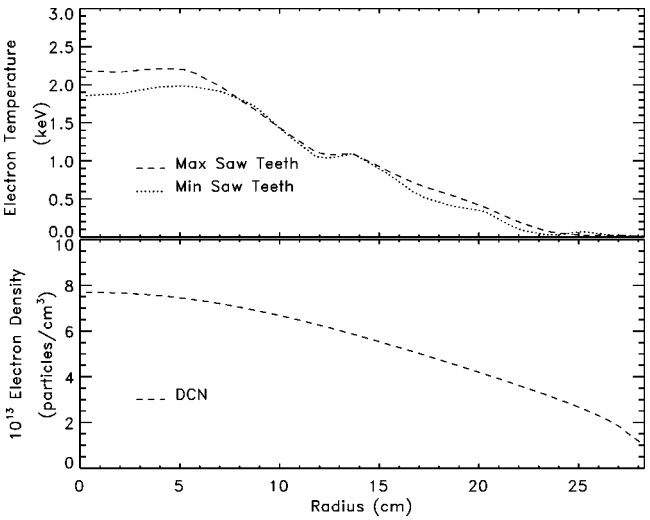

FIG. 2. Temperature and density profiles in FTU Tokamak plasmas for the LBO of Fe and the intrinsic Ni spectroscopic measurements.

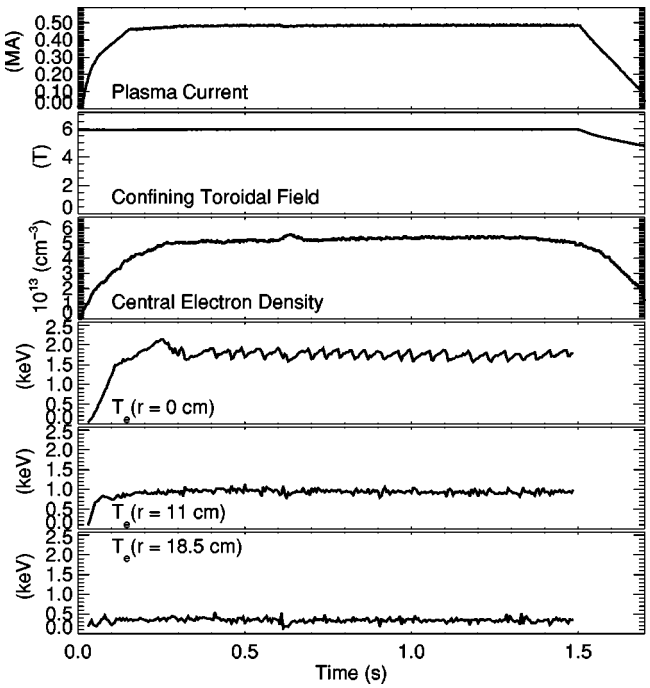

FIG. 3. Time history of an FTU plasma showing the plasma current, toroidal magnetic field, central electron density, and the electron temperature at three different radii. This plasma has an LBO of iron at 0.6 s.

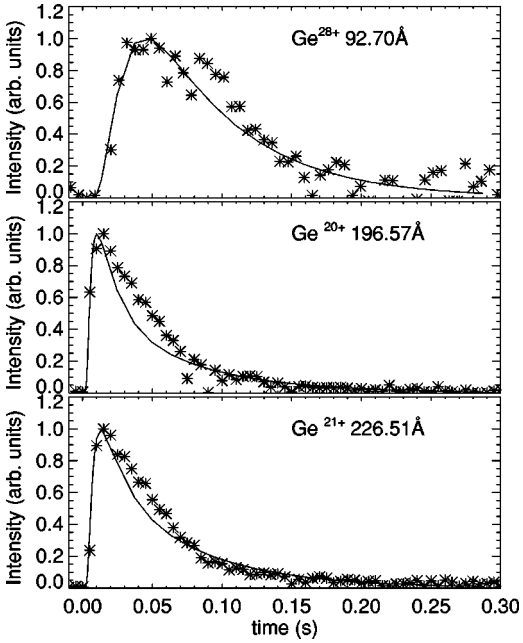

FIG. 4. Selected germanium time histories experimentally measured by the spectrometers with a central line of sight (**) and simulated by the MIST transport code using the rates from Mattioli *et al.* (—).

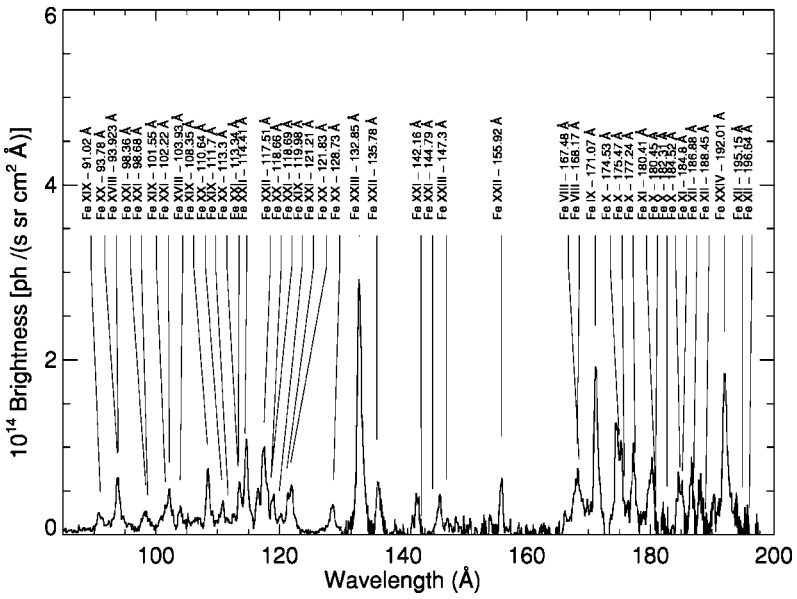

FIG. 5. Fe spectrum from GRITS between 85 to 200 Å during an LBO measured along a central line of sight at $t=0.61$ s.

through Ni, the computations were extended to include Cu to Ge [18]. The extension of the Mazzotta work will be referred to as the rates of Mattioli in this paper since he has performed the extrapolations.

Simulations with the ADPAK rates were inadequate to reproduce the profiles for Fe, Ge, and Ni. For Fe, agreement between the measured and simulated profiles for the Li-, Be-, Na-, and Mg-like ionization states was only possible with ionization/recombination rates from Arnaud and Raymond (AR92) or Mazzotta *et al.* The best simulations were possible with the compilations of Mazzotta *et al.* for Ni or Mattioli for Ge. The profiles of the F- to B-like charge states could not be reproduced by any of these atomic physics compilations. These charge states were found to exist at higher temperatures than predicted by the atomic physics rates. To get agreement between experiment and simulation, the dielectronic recombination rates of F→Ne-like to B→C-like needed to multiplied by a factor of ~ 2.

II. EXPERIMENT

During these experiments the FTU Tokamak (Fig. 1) operated with a plasma current, I_p, of 0.5 MA, a toroidal magnetic field B_T of 5.9 T, and an Ohmic input power P_{OH}, of ~ 1 MW. The plasma was circular with a major radius of 93 cm and a minor radius of 30 cm with a working gas of hydrogen. FTU has no divertor. The electron temperature was measured by Thomson scattering roughly every 50 ms and by electron cyclotron emission with a 5 ms temporal resolution. The electron density was determined with the far infrared radiation (FIR) laser or the DCN interferometer [19]. The density and temperature profiles are shown in Fig. 2 for the Fe and Ni experiments. Since Ni and Fe were measured during the same plasma, the temperature used for nickel is very similar to that during the LBO. For the Germanium experiments the central electron temperature was 2.7 keV with a similar profile to that shown in Fig. 2. The time history of a sample plasma is presented in Fig. 3 which includes the time evolution of the electron temperature at several different radii.

Three photometrically calibrated spectrometers measured the injected and intrinsic impurity emission and the spatial brightness profiles in the 1 to 1700 Å region. The XUV spectrograph (GRITS) was a 1 m Rowland circle, grazing incidence (at 2°) system with a 1200 grooves/mm gold coated grating [20,21]. The detector consisted of a microchannel plate-phosphor reticon [22]. The wavelength coverage was 10–350 Å with ~60 Å covered by the detector during each discharge. This instrument was photometrically calibrated using the SURF II synchrotron facility at the National Bureau of Standards and Technology (NIST) in August 1997. The error on the absolute photometric calibration was $\pm 20\%$.

The VUV spectrometer was a Survey, Poor Resolution, Extended Domain Spectrometer (SPRED) [23]. The longer wavelength grating had 290 grooves/mm and covered the 200–1700 Å range in each plasma. The shorter wavelength

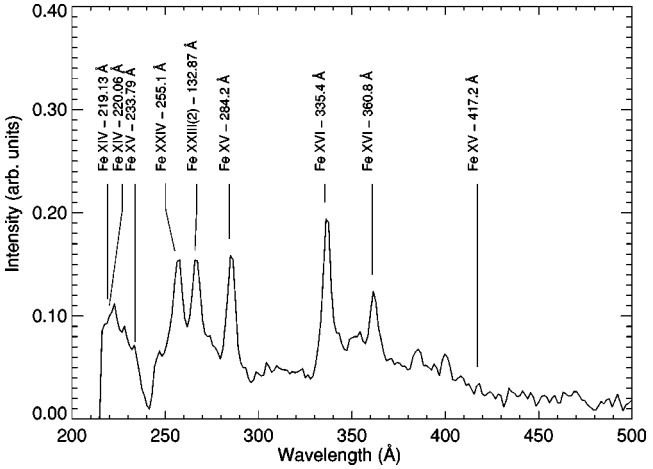

FIG. 6. Fe spectrum from SPRED between 200 to 500 Å during an LBO measured along a central line of sight at $t=0.61$ s.

TABLE I. Fe lines of interest in FTU Tokamak LBO experiments.

Ionization state	Isoelectronic sequence	Wavelength (Å)	Transition
Fe^{18+}	O-like	91.02	$1s^22s^22p^4$-$1s^22s2p^5$ ($^1D_2$-$^1P_1$)
Fe^{19+}	N-like	93.78	$1s^22s^22p^3$-$1s^22s2p^4$ ($^2D_{5/2}$-$^2P_{1/2}$)
Fe^{17+}	F-like	93.92	$1s^22s^22p^5$-$1s^22s2p^6$ ($^2S_{3/2}$-$^2P_{1/2}$)
Fe^{20+}	C-like	98.36	$1s^22s^22p^21s^22s2p^3$ ($^1D_2$-$^1P_1$)
Fe^{20+}	C-like	98.68	$1s^22s^22p^2$-$1s^22s^22p^3$ ($^1D_2$-$^1P_1$)
Fe^{18+}	O-like	101.55	$1s^22s^22p^4$-$1s^22s2p^5$ ($^3P_2$-$^3P_1$)
Fe^{20+}	C-like	102.22	$1s^22s^22p^2$-$1s^22s^22p^3$ ($^3P_2$-$^3S_1$)
Fe^{17+}	F-like	103.937	$1s^22s^22p^5$-$1s^22s2p^6$ ($^2S_{1/2}$-$^2P_{3/2}$)
Fe^{18+}	O-like	106.32	$1s^22s^22p^4$-$1s^22s2p^5$ ($^3P_1$-$^3P_0$)
Fe^{18+}	O-like	108.35	$1s^22s^22p^4$-$1s^22s2p^5$ ($^3P_2$-$^3P_2$)
Fe^{18+}	O-like	109.97	$1s^22s^22p^4$-$1s^22s2p^5$ ($^3P_0$-$^3P_1$)
Fe^{19+}	N-like	110.64	$1s^22s^22p^3$-$1s^22s2p^4$ ($^2D_{3/2}$-$^2D_{3/2}$)
Fe^{18+}	O-like	111.70	$1s^22s^22p^4$-$1s^22s2p^5$ ($^3P_1$-$^3P_1$)
Fe^{20+}	C-like	113.30	$1s^22s^22p^2$-$1s^22s^22p^3$ ($^1D_2$-$^1D_2$)
Fe^{19+}	N-like	113.34	$1s^22s^22p^3$-$1s^22s2p^4$ ($^2D_{5/2}$-$^2D_{5/2}$)
Fe^{21+}	B-like	114.41	$1s^22s^22p$-$1s^22s2p^2$ ($^2P_{3/2}$-$^2P_{3/2}$)
Fe^{21+}	B-like	116.26	$1s^22s^22p$-$1s^22s2p^2$ ($^2P_{3/2}$-$^2P_{1/2}$)
Fe^{21+}	B-like	117.17	$1s^22s^22p$-$1s^22s2p^2$ ($^2P_{1/2}$-$^2S_{1/2}$)
Fe^{20+}	C-like	117.51	$1s^22s^22p^2$-$1s^22s^22p^3$ ($^3P_1$-$^3P_1$)
Fe^{19+}	N-like	118.66	$1s^22s^22p^3$-$1s^22s2p^4$ ($^4S_{3/2}$-$^4P_{1/2}$)
Fe^{20+}	C-like	118.69	$1s^22s^22p^2$-$1s^22s^22p^3$ ($^3P_1$-$^3P_0$)
Fe^{18+}	O-like	119.98	$1s^22s^22p^4$-$1s^22s2p^5$ ($^3P_1$-$^3P_2$)
Fe^{20+}	C-like	121.21	$1s^22s^22p^2$-$1s^22s^22p^3$ ($^3P_2$-$^3P_2$)
Fe^{19+}	N-like	121.83	$1s^22s^22p^3$-$1s^22s2p^4$ ($^4S_{3/2}$-$^4P_{3/2}$)
Fe^{20+}	C-like	128.73	$1s^22s^22p^2$-$1s^22s^22p^3$ ($^3P_0$-$^3D_1$)
Fe^{22+}	Be-like	132.85	$1s^22s^2$-$1s^22s2p$ ($^1S_0$-$^1P_1$)
Fe^{19+}	N-like	132.85	$1s^22s^22p^3$-$1s^22s2p^4$ ($^4S_{3/2}$-$^4P_{5/2}$)
Fe^{21+}	B-like	135.78	$1s^22s^22p$-$1s^22s2p^2$ ($^2P_{1/2}$-$^2D_{3/2}$)
Fe^{20+}	C-like	142.16	$1s^22s^22p^2$-$1s^22s^22p^3$ ($^3P_1$-$^3D_2$)
Fe^{20+}	C-like	144.79	$1s^22s^22p^2$-$1s^22s^22p^3$ ($^1D_2$-$^1D_2$)
Fe^{21+}	B-like	155.92	$1s^22s^22p$-$1s^22s2p^2$ ($^2P_{3/2}$-$^2D_{5/2}$)
Fe^{23+}	Li-like	192.017	$1s^22s$-$1s^22p$ ($^2S_{1/2}$-$^2P_{3/2}$)
Fe^{23+}	Li-like	255.090	$1s^22s$-$1s^22p$ ($^2S_{1/2}$-$^2P_{3/2}$)
Fe^{14+}	Mg-like	284.147	$2p^63s^2$-$2p^63s3p$ ($^1S_0$-$^1P_1$)
Fe^{15+}	Na-like	335.407	$2p^63s$-$2p^63p$ ($^2S_{1/2}$-$^2P_{3/2}$)
Fe^{15+}	Na-like	360.798	$2p^63s$-$2p^63p$ ($^2S_{1/2}$-$^2P_{1/2}$)

grating had 2100 grooves/mm, and the wavelength coverage was nominally 100–300 Å. The SPRED calibration was directly transferred from the GRITS in the shorter wavelengths and extended to the longer wavelengths by the line ratio technique [24]. The error on the calibration was $\pm 35\%$ at 300 Å and was roughly a factor of 2 at 1000 Å. Both the VUV spectrometers could be positioned on a shot to shot basis to view the plasma from a minor radius of 0 to ~ 25 cm. This spatial range covered the majority of the interesting emission in the plasma.

The high resolution ($\lambda/\Delta\lambda > 10\,000$) bent crystal x-ray spectrometer [25] used the typical Johann configuration. A two-dimensional multiwire proportional chamber detector and a variable slit located between the crystal and the detector allowed a space resolved view of the plasma poloidal cross section. The crystal is a quartz Qz 220 that is bent so $2r = 6.5$ m. The operational angle Θ_B is 48.8° since $2d = 0.24565$ nm. The crystal length is 90 mm, and the height is 47 mm. The integrated reflectivity $R(i)$ is 6.58×10^{-6}. The spectrometer observed the K_α iron spectrum in the wavelength region between the $1s^2\,{}^1S_0$–$1s2p\,{}^1P_1$ resonance transition $\lambda(w) = 1.8500$ Å of the He-like ion and the $1s^22s^2\,{}^1S_0$–$1s2s^22p\,{}^1P_1$ transition $\lambda(b) = 1.8702$ Å of the Be-like ion. Line identification follows Gabriel's [26] and Bely-Dubau's [27] notation. This instrument measured the Fe profiles in a single shot. For Fe, the VUV measurements were normalized to the bent crystal measurements to remove any shot to shot uncertainties.

Fe and Ge were introduced into the plasma by LBO. Time histories of the Na-, Mg-, Be-like charge states as viewed with a central line of sight are plotted in Fig. 4 for a Ge LBO at 0.6 s in discharge 16805. For germanium, the Li-like line

TABLE II. Ni lines of interest in FTU Tokamak.

Ionization state	Isoelectronic sequence	Wavelength (Å)	Transition
Ni^{20+}	O-like	81.96	$1s^22s^22p^4$-$1s^22s2p^5$ ($^1D_2$-$^1P_1$)
Ni^{19+}	F-like	83.18	$1s^22s^22p^5$-$1s^22s2p^6$ ($^2S_{3/2}$-$^2P_{1/2}$)
Ni^{21+}	N-like	84.06	$1s^22s^22p^3$-$1s^22s2p^4$ ($^2D_{5/2}$-$^2P_{3/2}$)
Ni^{22+}	C-like	88.11	$1s^22s^22p^21s^22s2p^3$ ($^1D_2$-$^1P_1$)
Ni^{20+}	O-like	88.81	$1s^22s^22p^4$-$1s^22s2p^5$ ($^3P_2$-$^3P_1$)
Ni^{22+}	C-like	91.83	$1s^22s^22p^2$-$1s^22s^22p^3$ ($^3P_2$-$^3S_1$)
Ni^{20+}	O-like	93.91	$1s^22s^22p^4$-$1s^22s2p^5$ ($^3P_1$-$^3P_0$)
Ni^{19+}	F-like	94.50	$1s^22s^22p^5$-$1s^22s2p^6$ ($^2S_{1/2}$-$^2P_{3/2}$)
Ni^{20+}	O-like	95.85	$1s^22s^22p^4$-$1s^22s2p^5$ ($^3P_2$-$^3P_2$)
Ni^{20+}	O-like	96.79	$1s^22s^22p^4$-$1s^22s2p^5$ ($^3P_0$-$^3P_1$)
Ni^{21+}	N-like	98.16	$1s^22s^22p^3$-$1s^22s2p^4$ ($^2D_{3/2}$-$^2D_{3/2}$)
Ni^{18+}	O-like	100.23	$1s^22s^22p^4$-$1s^22s2p^5$ ($^3P_1$-$^3P_1$)
Ni^{21+}	N-like	100.61	$1s^22s^22p^3$-$1s^22s2p^4$ ($^2D_{5/2}$-$^2D_{5/2}$)
Ni^{22+}	C-like	102.08	$1s^22s^22p^2$-$1s^22s^22p^3$ ($^1D_2$-$^1D_2$)
Ni^{23+}	B-like	102.11	$1s^22s^22p$-$1s^22s2p^2$ ($^2P_{3/2}$-$^2P_{3/2}$)
Ni^{22+}	C-like	103.23	$1s^22s^22p^2$-$1s^22s^22p^3$ ($^3P_1$-$^3P_1$)
Ni^{21+}	N-like	103.31	$1s^22s^22p^3$-$1s^22s2p^4$ ($^4S_{3/2}$-$^4P_{1/2}$)
Ni^{23+}	B-like	103.53	$1s^22s^22p$-$1s^22s2p^2$ ($^2P_{3/2}$-$^2P_{1/2}$)
Ni^{23+}	B-like	104.64	$1s^22s^22p$-$1s^22s2p^2$ ($^2P_{1/2}$-$^2S_{1/2}$)
Ni^{22+}	C-like	106.02	$1s^22s^22p^2$-$1s^22s^22p^3$ ($^3P_2$-$^3P_2$)
Ni^{21+}	N-like	106.04	$1s^22s^22p^3$-$1s^22s2p^4$ ($^4S_{3/2}$-$^4P_{3/2}$)
Ni^{20+}	O-like	109.29	$1s^22s^22p^4$-$1s^22s2p^5$ ($^3P_1$-$^3P_2$)
Ni^{22+}	C-like	111.23	$1s^22s^22p^2$-$1s^22s^22p^3$ ($^3P_1$ $^3P_0$)
Ni^{22+}	C-like	111.86	$1s^22s^22p^2$-$1s^22s^22p^3$ ($^3P_0$-$^3D_1$)
Ni^{24+}	Be-like	117.91	$1s^22s^2$-$1s^22s2p$ ($^1S_0$-$^1P_1$)
Ni^{21+}	N-like	117.91	$1s^22s^22p^3$-$1s^22s2p^4$ ($^4S_{3/2}$-$^4P_{5/2}$)
Ni^{23+}	B-like	118.52	$1s^22s^22p$-$1s^22s2p^2$ ($^2P_{1/2}$-$^2D_{3/2}$)
Ni^{22+}	C-like	126.54	$1s^22s^22p^2$-$1s^22s^22p^3$ ($^3P_1$-$^3D_2$)
Ni^{22+}	C-like	128.87	$1s^22s^22p^2$-$1s^22s^22p^3$ ($^1D_2$-$^1D_2$)
Ni^{23+}	B-like	138.80	$1s^22s^22p$-$1s^22s2p^2$ ($^2P_{3/2}$-$^2D_{5/2}$)
Ni^{25+}	Li-like	165.42	$1s^22s$-$1s^22p$ ($^2S_{1/2}$-$^2P_{3/2}$)
Ni^{25+}	Li-like	234.20	$1s^22s$-$1s^22p$ ($^2S_{1/2}$-$^2P_{3/2}$)
Ni^{16+}	Mg-like	249.180	$2p^63s^2$-$2p^63s3p$ ($^1S_0$-$^1P_1$)
Ni^{17+}	Na-like	291.977	$2p^63s$-$2p^63p$ ($^2S_{1/2}$-$^2P_{3/2}$)
Ni^{17+}	Na-like	320.537	$2p^63s$-$2p^63p$ ($^2S_{1/2}$-$^2P_{1/2}$)

at 122.6 Å is blended with an *M*-shell emission line. The temperature of the plasma was too low to produce sufficient quantities of the Li-like charge state to overcome this blending problem. This Li-like ion was observed in auxiliary heated plasmas with $T_e \sim 6.5$ keV. For iron and nickel the plasma was hot enough to easily produce the Li-like charge state. Nickel was observed as an intrinsic impurity which was sputtered from the inconel limiter. Its concentration was constant during the plasma current steady state and on a shot to shot basis during these experiments. The n_0(Fe) was $\sim 4\times10^{11}$ particles/cm^3, n_0(Ni) was $\sim 1\times10^{11}$ particles/cm^3, and n_0(Ge)$\sim 4\times10^{11}$ particles/cm^3. The other major high *Z* impurity was molybdenum which has been previous studied on FTU [8].

The measurement of each spatial brightness profile required 10–15 similar plasmas during which the spectrometers were scanned spatially on a shot to shot basis. Sample Fe spectra are shown in Figs. 5 and 6 from the GRITS and the SPRED at the peak of the LBO with a central line of sight. The iron, germanium, and nickel emission lines are summarized in Tables I, II, and III. The wavelengths are those published in Ref [28]. From the spectra obtained during the spatial scans of the spectrometers, the spatial brightness profiles of the major radiating charge states were obtained as a function of time. The measured profiles (shown as points) at 40 ms after the LBO or at 0.64 s from the start of the plasma are presented in Fig. 7 for Fe^{14+} (Mg-like), Fe^{15+}, Fe^{22+}, and Fe^{23+}; in Fig. 8 for Fe^{17+} (F-like), Fe^{18+}, Fe^{19+}, Fe^{20+}, and Fe^{21+}; and in Fig. 9 for Fe^{24+} (He-like). The germanium profiles are shown in Fig. 10 for Ge^{20+}, Ge^{21+}, and Ge^{28+}; and in Fig. 11 for Ge^{24+} (O-like), Ge^{25+}, Ge^{26+}, and Ge^{27+}. The nickel profiles are shown in Fig. 12 for Ni^{16+} (Mg-like), Ni^{17+}, Ni^{24+}, and Ni^{25+}; and in Fig. 13 for Ni^{19+} (F-like), Ni^{20+}, Ni^{21+}, Ni^{22+}, and Ni^{23+}. The error

TABLE III. Ge lines of interest in FTU Tokamak LBO experiments.

Ionization state	Isoelectronic sequence	Wavelength (Å)	Transition
Ge^{25+}	F-like	65.90	$1s^22s^22p^5$-$1s^22s2p^6$ ($^2P_{3/2}$-$^2S_{1/2}$)
Ge^{24+}	O-like	68.61	$1s^22s^22p^4$-$1s^22s2p^5$ ($^3P_2$-$^3P_1$)
Ge^{26+}	C-like	70.67	$1s^22s^22p^2$-$1s^22s2p^3$ ($^3P_1$-$^3S_1$)
Ge^{24+}	O-like	75.21	$1s^22s^22p^4$-$1s^22s2p^5$ ($^3P_0$-$^3P_1$)
Ge^{24+}	O-like	75.51	$1s^22s^22p^4$-$1s^22s2p^5$ ($^3P_2$-$^3P_2$)
Ge^{25+}	N-like	78.56	$1s^22s^22p^3$-$1s^22s2p^4$ ($^4S_{3/2}$-$^4P_{1/2}$)
Ge^{25+}	N-like	78.70	$1s^22s^22p^3$-$1s^22s2p^4$ ($^2D_{3/2}$-$^2D_{3/2}$)
Ge^{25+}	N-like	79.64	$1s^22s^22p^3$-$1s^22s2p^4$ ($^2D_{5/2}$-$^2D_{5/2}$)
Ge^{25+}	N-like	80.08	$1s^22s^22p^3$-$1s^22s2p^4$ ($^4S_{3/2}$-$^4P_{3/2}$)
Ge^{26+}	C-like	81.4	$1s^22s^22p^2$-$1s^21s^22s2p^3$ ($^3P_1$-$^3P_0$)
Ge^{26+}	C-like	83.21	$1s^22s^22p^2$-$1s^22s2p^3$ ($^1D_2$-$^1D_2$)
Ge^{27+}	B-like	83.5	$1s^22s^22p$-$1s^22s2p^2$ ($^2P_{1/2}$-$^2S_{1/2}$)
Ge^{26+}	C-like	85.12	$1s^22s^22p^2$-$1s^22s2p^3$ ($^3P_0$-$^3D_1$)
Ge^{27+}	B-like	90.64	$1s^22s^22p$-$1s^22s2p^2$ ($^2P_{1/2}$-$^2D_{3/2}$)
Ge^{25+}	N-like	92.18	$1s^22s^22p^3$-$1s^22s2p^4$ ($^4S_{3/2}$-$^4P_{5/2}$)
Ge^{28+}	Be-like	92.7	$1s^22s^2$-$1s^22s2p$ ($^1S_0$-$^1P_1$)
Ge^{24+}	O-like	92.53	$1s^22s^22p^4$-$1s^22s2p^5$ ($^3P_1$-$^3P_2$)
Ge^{29+}	Li-like	122.6	$1s^22s$-$1s^22p$ ($^2S_{1/2}$-$^2P_{3/2}$)
Ge^{13+}	K-like	122.82	$2p^63s^23p^63d$-$2p^63s^23p^53d^2$ ($^2D_{5/2}$-$^2F_{7/2}$)
Ge^{29+}	Li-like	200.1	$1s^22s$-$1s^22p$ ($^2S_{1/2}$-$^2P_{1/2}$)
Ge^{20+}	Mg-like	196.57	$2p^63s^2$-$2p^63s3p$ ($^1S_0$-$^1P_1$)
Ge^{21+}	Na-like	226.505	$2p^63s$-$2p^63p$ ($^2S_{1/2}$-$^2P_{3/2}$)
Ge^{21+}	Na-like	261.52	$2p^63s$-$2p^63p$ ($^2S_{1/2}$-$^2P_{1/2}$)
Ge^{20+}	Mg-like	293.4	$2p^63s^2$-$2p^63s3p$ ($^1S_0$-$^3P_1$)

bars on the experimental points are the uncertainties on the absolute photometric calibration. The simulations (lines) with the different sets of atomic physics rates are discussed in the following sections.

The anomalous impurity particle transport for ohmically heated plasmas was determined from the LBO's and from visible bremsstrahlung emission [29,30]. The transport was characterized by a diffusion D and a convective velocity $V(r)=-2SDr/a^2$. The value S, the peaking factor, is a dimensionless multiplier of the convective velocity. A detailed discussion of the transport analysis can be found for non intrinsic Kr and Ar which were introduced into FTU plasmas for atomic physics studies [7]. The τ_p from these injections was $\sim$35 ms in ohmically heated plasmas. The particle transport was determined to be $D=5000$ cm^2/s with $S=1$. This method was an independent estimation of the particle transport since it did not depend upon the measurements from the spectrometers. Therefore, the only unknown in the simulations was the set of atomic physics rates.

III. ATOMIC PHYSICS MODEL AND RATES

The calculation of the charge state distribution of various ion stages of astrophysically abundant elements up to and including Ni is often the first step in understanding the emission from hot astrophysical plasmas. Moreover, the rate coefficients for collisional ionization and recombination required for equilibrium calculations are crucial for the nonequilibrium modeling. Calculations of these rates are performed by atomic physicists and new detailed results which are mainly (but not only) theoretical are quite frequently published. It is then necessary to periodically review the literature and to assess the proposed rates for evaluating new charge state distributions. Both the assessed rates and the assessed fractional abundances are available to astrophysicists. In the 1970s these ''reference'' evaluations were those by Jordan [31,32]. In the 1980's the published works are by Shull and Van Steenberg [33] and by AR85. AR92 is a critical review of the ionization and recombination rates for only Fe. The new CSD's were evaluated and compared with the corresponding older AR85 CSD's. Non-negligible differences were reported, as apparent in their Figs. 11 and 12. Recently Mazzotta *et al.* did the same assessment as AR92 for all the elements up to Ni. In their figures they compare their CSDs with those proposed by AR85, AR92, and also for elements not considered by AR85, with those proposed by Landini and Monsignori Fossi [34].

Impurity behavior in MCF devices are simulated by numerical modeling codes using some subset of the ionization and recombination rates mentioned above. For our analysis of reported FTU experimental data the multiple ionization state transport (MIST) [17] code was used. The original rates in MIST were those from AdPak from the late 1970's. The electron impact ionization rates in ADPAK included direct impact (DI) ionization computed using the formula of Lotz [35], but not excitation-autoionization (EA) rates. The ADPAK recombination processes included both radiative recombination (RR) and dielectronic recombination (DR), the latter be-

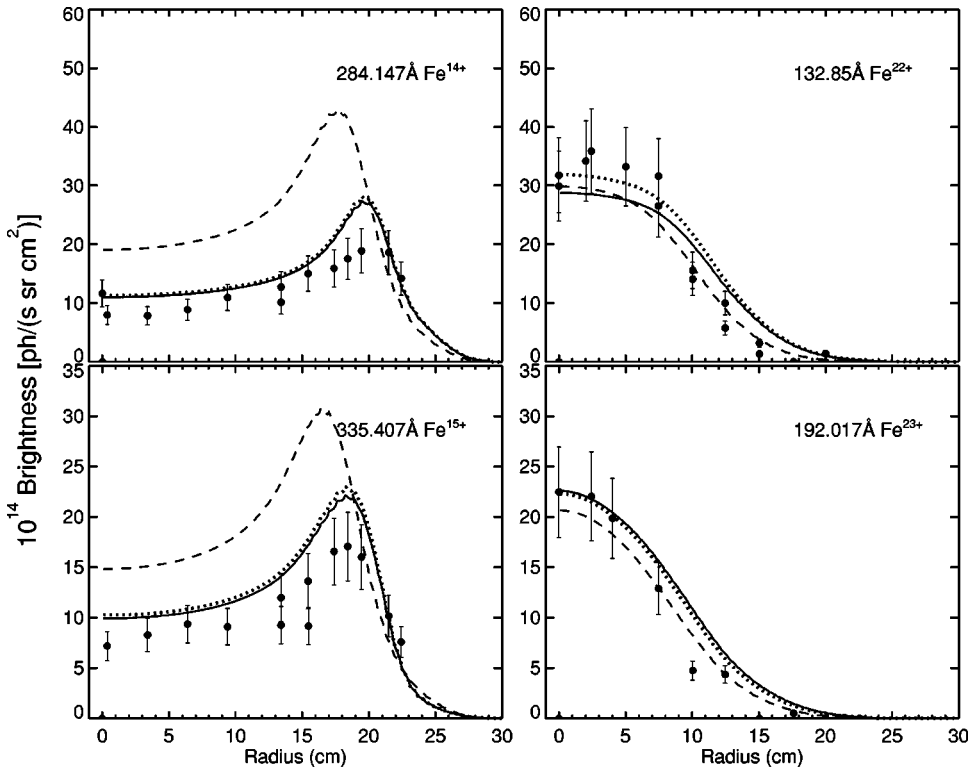

FIG. 7. Experimental and modeled spatial brightness profiles of the Fe^{14+} (Mg-like), Fe^{15+}, Fe^{22+}, and Fe^{23+} lines at 0.64 s during an LBO. Plotted are simulations using three sets of atomic physics rates ($\cdots$: AR92, —: Mazzotta *et al.*, - - -: ADPAK).

ing approximated by the formulas of Burgess and Mertz [36–38].

The MIST code and a collisional radiative (CR) model were used to simulate the time evolution and spatial brightness profiles of the LBO's of Ge and Fe and the spatial profiles of intrinsic Ni. This analysis determined the best choice of the atomic physics rate compilations. MIST is a one-dimensional (radial in cylindrical coordinates) time dependent impurity transport code which treats the ionization/recombination physics and the trace impurity particle transport simultaneously. Inputs into MIST were the experimentally measured radial electron temperature profile (Figs. 2 and 3), the electron density profile, the particle transport parameters, and the impurity concentration. The transient nature of the LBO's of Fe and Ge required a time dependent simulation of the impurity dynamics. A time dependent temperature profile was used since the LBO slightly perturbed the edge temperature, and the core plasma was affected by saw teeth oscillations. Time independent simulations were run for Ni since its concentration during the plasmas was constant. MIST outputs the fractional abundance of each ionization state in the plasma as a function of time with a given set of ionization/recombination rates. Simulations were run with the compilations of ADPAK, Arnaud and Raymond (AR92), Arnaud and Rothenflug (AR85), Mazzotta *et al.*, and Mattioli (the extension of the Mazzotta rates for Cu through Ge). Since the compliation of AR85 included H to Ni, the germanium simulations were preformed with only ADPAK and Mattioli rate coefficients.

Collisional excitation rates and photodecay rates provided by HULLAC and the CSD provided by the MIST code were incorporated into the CR model which determined the intensities for each emission line of interest. The emissivity of each line was calculated for each radial magnetic flux surface of the circular FTU plasma. The flux surfaces used in the MIST were on a grid of 50 points between $r/a=0$ to 1.1 separated equally in radius. These emissivities were summed over the line of sight of the spectrometers to produce the synthetic brightness profiles for intrinsic nickel. The procedure was performed as a function of time for the Fe and Ge LBOs. A synthetic brightness profile was generated for each compilation of ionization/recombination physics rates used for comparison with experiment.

IV. TIME HISTORIES AND SPATIAL PROFILES

A. Time histories

As mentioned, the measured and simulated time evolutions of the several germanium charge states are presented in Fig. 4 during the LBO into FTU ohmically heated shot 16 805. The points are the experimental measurements of the Ge^{20+} (Mg-like), Ge^{21+}, and Ge^{28+} (Be-like: core) ionization states. In this plasma the electron temperature was insufficient to produce measurable quantities of Ge^{29+}. The germanium penetrated to the core very quickly within 5 ms. After reaching a maximum the brightnesses and the impurity concentration decayed exponentially for all the ionization states. The lowest charge states which emitted from shells near the edge peaked first and quickly decayed after entering the plasma. The highest charge states which existed in the core peaked much later. The temporal response of each charge state was affected by both the ionization/recombination physics and the particle transport. The emission lines simulated with the Mattioli rates are plotted as solid lines and were in agreement with the experiment.

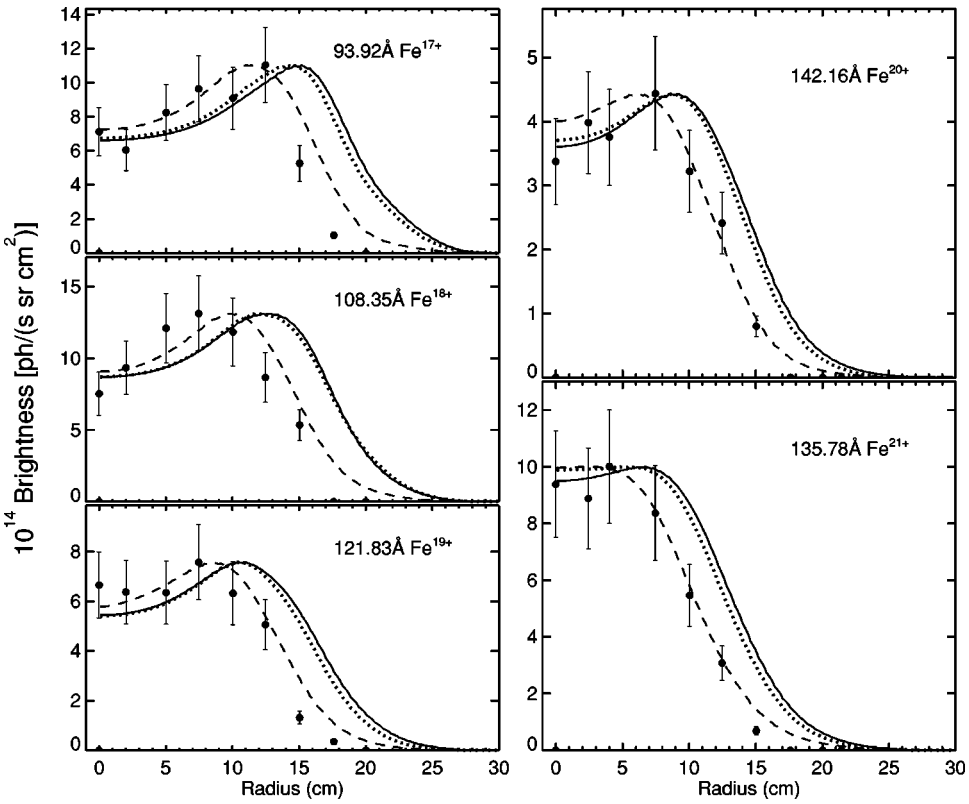

FIG. 8. Experimental and modeled spatial brightness profiles of the Fe^{17+} (F-like), Fe^{18+}, Fe^{19+}, Fe^{20+}, and Fe^{21+} lines at 0.64 s during an LBO. Plotted are simulations using three sets of atomic physics rates (· · ·: AR92, —: Mazzotta *et al.*, - - -: Adjusted rates).

For Fe, the core (Li- and Be-like) states are well simulated quantitatively, but the simulations of the outer states (Na- and Mg-like) are only in qualitative agreement. The simulated final decay of these states was correct in time and in absolute magnitude, but the simulated initial inflow was more intense and steep than that observed. The discrepancy is thought to result from the choice of boundary conditions and the impurity source at the very edge of the plasma. The source is considered to be a delta function in all these simulations, since no measurement was available. The corresponding Ge charge states existed farther from the edge of the plasma and are much less affected than those of Fe. To eliminate any problems with the particle inflow and the LBO source, the spatial brightness profiles presented for iron and germanium are taken during the decay phase of the impurity just after the peak of the highest charge state [$t(\mathrm{LBO}) = +40$ ms, $t(\mathrm{plasma}) = 640$ ms].

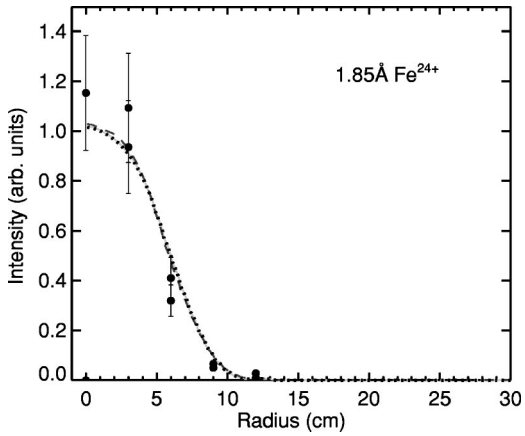

FIG. 9. Experimental and modeled spatial brightness profiles of the Fe^{24+} line at 0.64 s during an LBO. Plotted are simulations using three sets of atomic physics rates (· · ·: AR92, —: Mazzotta *et al.*, - - -: ADPAK).

B. Iron profiles

The spatial brightness profile simulations are compared to the experimentally measured points for Fe^{14+} (Mg-like), Fe^{15+}, Fe^{22+}, and Fe^{23+} in Fig. 7; for Fe^{17+} (F-like), Fe^{18+}, Fe^{19+}, Fe^{20+}, and Fe^{21+} in Fig. 8; and for Fe^{24+} (He-like) in Fig. 9. These profiles were obtained during FTU shots 16 771–16 792. All the simulations in Fig. 7 are normalized to the Li/Be-like charge states. Each simulation in Fig. 8 is normalized to the maximum experimental point for each emission line. In Fig. 9 the units are in arbitrary units because an unresolvable calibration discrepancy exists between the x-ray and the VUV spectrometers. The difference is roughly two orders of magnitiude. Only a qualitative agreement is possible for Fe^{24+}.

The simulated brightness profiles with the Mazzotta *et al.* (solid lines) and AR92 (dotted lines) rates agree very well with the measured points for the five charge states Fe^{14+} (Mg-like), Fe^{15+}, Fe^{22+}, Fe^{23+}, and Fe^{24+}. Even though the simulations with the AR92 and Mazzotta *et al.* rates slightly overestimate the absolute magnitude of the emission for the Na- and Mg-like states, the position of the emitting peak is correctly modeled. The AR92 and Mazzotta *et al.* rates yield very similar results, which are much better than those using the ADPAK physics rates (dashed lines). Not only do the ADPAK rates fail to predict the absolute magnitude of the emis-

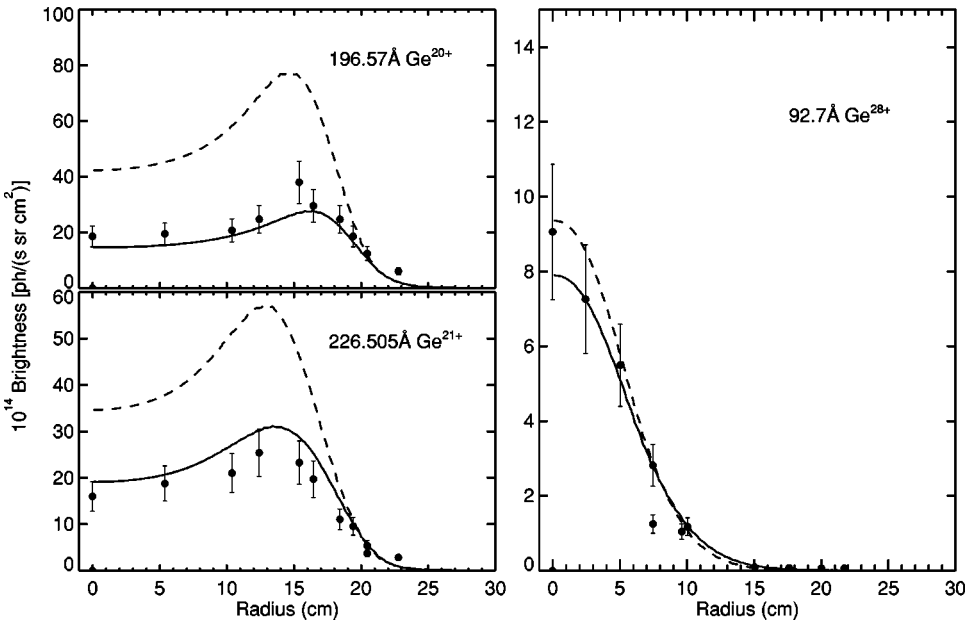

FIG. 10. Experimental and modeled spatial brightness profiles of the Ge^{20+}, Ge^{21+}(Na-like), and Ge^{28+} lines. Plotted are simulations using two sets of atomic physics rates (—: Mattioli, - - -: ADPAK).

sion of the Na- and Mg-like states, but cannot accurately simulate the radial position (temperature) of these emission peaks.

The F-like to B-like charge states in Fig. 8 are not well simulated by any of the atomic physics compilations. Both the magnitude and the spatial location of each line brightness are incorrectly simulated. The position of each emission feature is most important since it is a direct measure of the ionization/ recombination rates for the $\Delta n=0$ line brightness. The $\Delta n=0$ emission lines do not have significant temperature sensitivity in this region. The magnitude of the brightness is a function of the collisional excitation and the ionization/ recombination rates. To clearly show the discrepancies in the shape of the simulations in Fig. 8, each was normalized to the maximum experimental value of each emission line. The absolute magnitude of the measurement was a factor of 30% higher than the simulation for Fe^{21+} and increased to a factor of ~ 4 for Fe^{17+}. The simulated profile for the Fe^{21+} is at a slightly larger radius (lower temperature) than that observed. This is a consistent trend throughout the

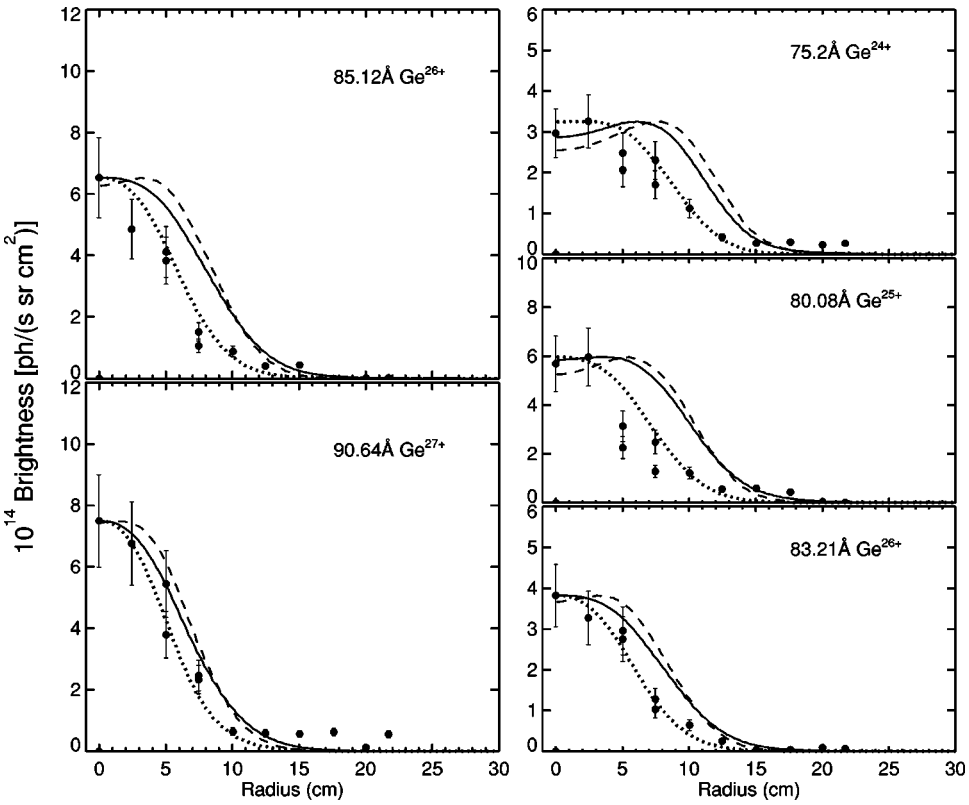

FIG. 11. Experimental and modeled spatial brightness profiles of the Ge^{24+} (O-like), Ge^{25+}, Ge^{26+}, and Ge^{27+} lines. Plotted are simulations using three sets of atomic physics rates (—: Mattioli, - - -: ADPAK, · · ·: adjusted rates).

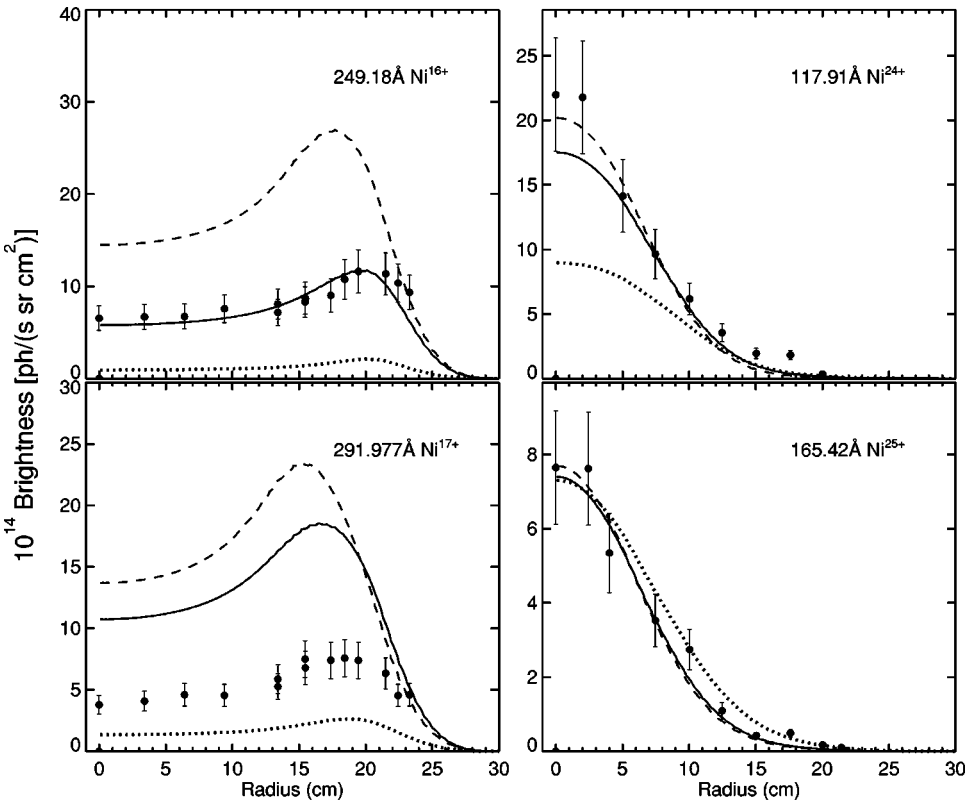

FIG. 12. Experimental and modeled spatial brightness profiles of the Ni^{16+} (Mg-like), Ni^{17+}, Ni^{24+}, and Ni^{25+} lines for intrinsic nickel. Plotted are simulations using three sets of atomic physics rates (···: AR85, —: Mazzotta *et al.*, - - -: ADPAK).

entire *L* shell. The discrepancy increases with charge state and is most significant for Fe^{17+}. Therefore, the shell of the Ne-like charge state should be much broader spatially and higher in temperature than would be predicted by these rates. Unfortunately, this cannot be confirmed because the Ne-like charge state could not be measured in these experiments due to the poor response of the spectrometers in the 10 Å range.

The level of inadequacy of the atomic physics rates was investigated by adjusting the DR rates for (F-like) $Fe^{17+} \rightarrow Fe^{16+}$ to (B-like) $Fe^{21+} \rightarrow Fe^{20+}$ in the simulations. Agree-

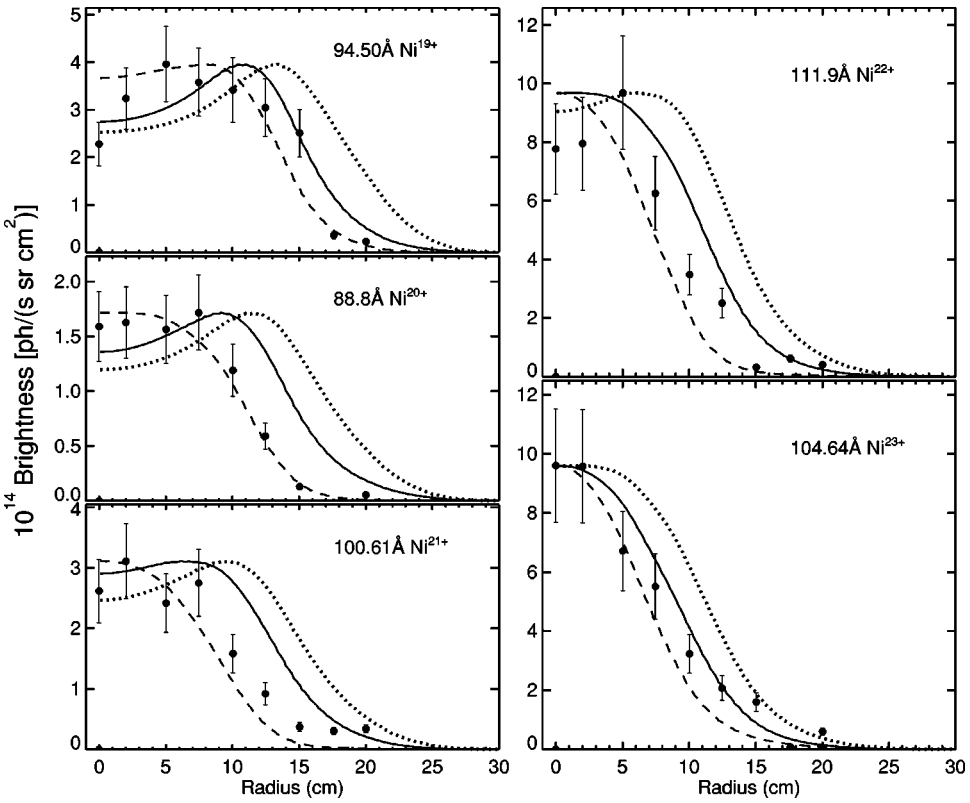

FIG. 13. Experimental and modeled spatial brightness profiles of the Ni^{19+} (F-like), Ni^{20+}, Ni^{21+}, Ni^{22+}, and Ni^{23+} lines for intrinsic nickel. Plotted are simulations using three sets of atomic physics rates (···: AR85, —: Mazzotta *et al.*, - - -: adjusted rates).

TABLE IV. Experimental and simulated line ratios for Li and Be-like Ge during ECRH heated plasmas with $T_e(0)$ of 6.5 keV.

Emission line	Experiment [ph/(s sr cm^2)]	Mattioli [ph/(s sr cm^2)]	ADPAK [ph/(s sr cm^2)]
Ge^{29+} 122.6 Å	5.00	4.89	5.25
Ge^{28+} 92.7 Å	10.73	10.42	10.59
Ratio	0.47	0.47	0.50

ment with the shape of the experimental profiles was only possible when these DR rates were multiplied by a factor of 2 as shown by the dashed lines in Fig. 8. With the altered DR rates, the simulated brightnesses of the B- and C-like states were changed by less than 20%. The simulated brightnesses of the N, O, and F-like states increased by factor of 1.5 to 2. Using the adjusted rates, it is possible to simulate the shape of the experimental profiles but not the brightesses.

The problem with the rates was thought to be with the DR rates and not the RR or ionization rates. From the Ne-like ions, in the direction of increasing ionization, the ionization rates were all calculated with a Younger-like formula [39] so that significant changes were not expected for neighboring ions. The DR rate calculations for each species have been treated with separate formulas, therefore, abrupt changes were more likely. This level of uncertainty in the atomic physics rates for these ions is not unreasonable and has been seen by others [40] but may not be the only reason for the discrepancy.

Both the measured temperature profile and the particle transport could also affect the simulated profiles of the F- to B-like charge states. Their effect on the simulations was investigated to eliminate them as possible causes of the discrepancy. The central electron temperature was reduced to 1.4 keV. With this temperature, the simulations using the Mazzotta rates were able to correctly predict the shape of the F- to B-like charge states. However, a 1.4 keV central temperature is unrealistic since the error bar on the TSC measurement is less than 100 eV in the core. Also, the ratio of the Li to Be-like emission lines were not correctly predicted. The Li-like line intensity is under predicted by a factor of ~ 2. Therefore, the temperature can be eliminated as a possible cause.

The particle transport has been measured to be 5000 cm^2/s in the core. An increase of the particle transport in the outer half of the plasma would shift the F-like to B-like ionization states to higher temperatures in the simulations. The peaking factor S was increased from 1 to 10 in one simulation (a) and the diffusion for $r/a > 0.5$ was increased from 5000 to 100 000 in another (b). With this increase in the particle transport, the spatial positions of the F- to B-like ionization states were correctly simulated. This level of transport is not consistent with the estimates on FTU. Furthermore, with either of these particle transports [(a) or (b)], the simulations cannot not reproduce the spatial profiles of the Na- and Mg-like charges states. If this transport is correct then the atomic physics for Na and Mg-like iron is incorrect. Therefore, the resulting conclusion is the same: A problem exists with the atomic physics rates for some of the charge states of iron (most likely the F- to B-like) which discrepancies in the transport or the temperature profile cannot explain.

C. Germanium profiles

The spatial brightness profile simulations are compared to the experimentally measured points for Ge^{20+} (Mg-like), Ge^{21+}, and Ge^{28+} in Fig. 10 and Ge^{24+} (O-like), Ge^{25+}, Ge^{26+}, and Ge^{27+} in Fig. 11. These profiles were obtained during FTU shots 16 805–16 821. The simulations used the atomic physics rates from ADPAK and Mattioli. The simulations in Fig. 11 have been normalized as describe above for Fe. The results are very similar for those of iron. The ADPAK rates are in general a poor choice for simulating Ge. The rates from Mattioli can be used successfully to simulate the Na-, Mg-, and Be-like charge states. The simulations of the B- to O-like ionization states required an enhancement of the relevant DR rates from Mattioli by a factor of ~ 2 in order to get the agreement shown by the dotted lines in Fig. 11. As with Fe, the shape of the emission feature is correct but not the absolute magnitude. The F-like charge is not shown since it was not within the measurement range of the spectrometers during these experiments.

The final experiment investigated the ratio of the Li-like line at 122.6 Å to the Be-like line at 92.7 Å. As previously stated, the temperature in the ohmic plasmas was insufficient to produce sufficient Li-like ions. To obtain higher temperatures the plasma was heated with auxiliary ECRH to produce 6.5 keV in the plasma core during shot 17902. Germanium was injected and the time histories were simulated with MIST. The results are listed in Table IV. As seen with iron, the simulations with the Mattioli and the ADPAK rates correctly predicted the ratio of the Li to the Be charge states, but the Mattioli rates give a slightly better agreement.

D. Nickel profiles

The analysis of steady state, intrinsic nickel did not have the complexity of the time dependent LBO simulations. Unfortunately, the first attempt to simulate the experimental profiles of Ni^{16+} (Mg-like), Ni^{17+}, Ni^{24+}, and Ni^{25+} in Fig. 12 did not have as good agreement as those for Fe. This implied that neither the AR85 nor Mazzotta rates adequately simulated the experiment. The discrepancy was found to be in the transport used for the intrinsic impurities. To determine the correct transport of intrinsic impurities, the Mazzotta atomic physics was assumed to be correct. The profiles of Fe^{14+} (Mg-like), Fe^{15+}, Fe^{22+}, and Fe^{23+} for intrinsic iron were measured after the iron LBO and modeled with the Mazzotta atomic physics. With $S = 2.5$, the simulations correctly reproduced the Fe experimental profiles. The nickel

profiles were simulated with $S=2.5$ and are shown in Fig. 12. The profiles for the core charge states were correctly simulated by the rates of Mazzotta *et al.* and ADPAK. The simulations using the rates of AR85 under predicted Be-like ion by a factor of 2. ADPAK rates did not predict the magnitude nor the spatial position for the Na- and Mg-like states. Both the AR85 and Mazzotta *et al.* rates correctly predicted the spatial positions. However, only the Mazzotta rates properly predicted the magnitude of the Mg-like ionization state and over predicted the Na-like ionization state by ~ 2. The Na- and Mg-like emission lines were weaker than the equivalent lines during the LBO of Fe. Since the nickel was intrinsic, blending of one of the lines with another intrinsic impurity cannot be completely eliminated. Their absolute intensities were less certain and, thus, can partly explain this discrepancy. We conclude that the Mazzotta rates are the best choice for simulating the spatial profiles of these ionization states.

The intermediate states Ni^{19+} (F-like), Ni^{20+}, Ni^{21+}, Ni^{22+}, and Ni^{23+} are shown in Fig. 13. The simulations have been normalized as described above for Fe. The Mazzotta *et al*. rates are a better choice, however, neither the AR85 nor the Mazzotta *et al.* compilations properly simulated the spatial positions. As with the iron simulations, the Mazzotta *et al*. DR rates for the B- to O-like ionization states were adjusted until the simulations matched experiment. The DR rates must be multiplied by ~ 2 to recover the experiment.

V. CONCLUSION

Fe and Ge were introduced into FTU Tokamak plasmas by the LBO technique to validate ionization/recombination atomic physics rates used to determine the CSD. Ni was an intrinsic impurity. Both the *L*- and *M*-shell spectrum of these elements have been measured by photometrically calibrated spectrometers in the 1–1700 Å region. The spatial brightness profiles of specific emission lines have been obtained in a set of similar ohmically heated plasmas. The MIST impurity transport code simulated the spatial brightness profiles with different sets of atomic physics rates. The atomic physics rates chosen for this work included the compliations of ADPAK [13], Mazzotta *et al*. [1], AR85 [2], AR92 [3], and Mattioli [18], an extension of Mazzotta from Cu to Ge. The Mattioli (for Ge), Mazzotta *et al*. (for Ni and Fe), and the AR92 rates (for Fe) adequately simulated the He- (Fe only), Li-, Be-, Na-, and Mg-like ionization states. The F- to B-like charge states could not be simulated by these compilations unless the relevant DR rates were multiplied by a factor of 2. The ADPAK rates could not be used to adequately predict any of charge states of Fe, Ge, or Ni.

ACKNOWLEDGMENTS

The authors would like to thank the entire FTU staff for their expert operation of the tokamak and the use of their facilities. We also thank the Princeton Plasma Physics Laboratory for use of the MIST transport code. This work is supported by U.S. DOE Grant No. DE-FG02-86ER53214 at JHU and was performed under the auspices of the U.S. Department of Energy by the University of California, Lawrence Livermore National Laboratory under contract No. W-7405-Eng-48.

[1] P. Mazzotta, G. Mazzitelli, S. Colafrancesco, and N. Vittorio, Astron. Astrophys., Suppl. Ser. **133**, 403 (1998).
[2] M. Arnaud and R. Rothenflug, Astron. Astrophys., Suppl. Ser. **60**, 425 (1985).
[3] M. Arnaud and J. Raymond, Astrophys. J. **398**, 394 (1992).
[4] J.E. Rice, J.L. Terry, K.B. Fournier, M.A. Graf, M. Finkenthal, M.J. May, E.S. Marmar, W.H. Goldstein, and A.E. Hubbard, J. Phys. B **29**, 2191 (1995).
[5] K.B. Fournier, W.H. Goldstein, A.L. Osterheld, M. Cohen, M. Finkenthal, M.J. May, J.L. Terry, M.A. Graf, and J. Rice, Phys. Rev. A **54**, 3870 (1996).
[6] K.B. Fournier *et al.*, Nucl. Fusion **40**, 847 (2000).
[7] M.J. May *et al.*, Phys. Rev. E **61**, 3042 (2000).
[8] D. Pacella, K.B. Fournier, M. Zerbini, M. Finkenthal, M. Mattioli, M.J. May, and W.H. Goldstein, Phys. Rev. E **61**, 5701 (2000).
[9] K.B. Fournier, M. Cohen, M.J. May, and W.H. Goldstein, At. Data Nucl. Data Tables **70**, 231 (1998).
[10] A. Bar-Shalom, M. Klapisch, and J. Oreg, Phys. Rev. A **38**, 1773 (1988).
[11] M. Klapisch, Comput. Phys. Commun. **2**, 269 (1971).
[12] M. Klapisch, J. Opt. Soc. Am. **67**, 148 (1977).
[13] D.E. Post, R.V. Jensen, C.B. Tarter, W.H. Grasberger, and W.A. Lokke, At. Data Nucl. Data Tables **20**, 397 (1977).
[14] P. Buratti, E. Barbato, G. Bracco, S. Cirant, F. Crisanti, G. Granucci, A.A. Tuccillo, V. Zanza, M. Zerbini, L. Acitelli, F. Alladio, B. Angelini, M.L. Apicella, G. Apruzzese, L. Bertalot, A. Bertocchi, M. Borra, A. Bruschi, G. Buceti, A. Cardinali, C. Centioli, R. Cesario, C. Cianfarani, S. Ciattaglia, V. Cocilovo, R. De Angelis, F. De Marco, B. Esposito, D. Frigione, L. Gabellieri, G. Gatti, E. Giovannozzi, C. Gourlan, M. Grolli, A. Imparato, H. Kroegler, M. Leigheb, L. Lovisetto, G. Maddaluno, G. Maffia, M. Marinucci, G. Mazzitelli, P. Micozzi, F. Mirizzi, S. Nowak, F.P. Orsitto, D. Pacella, L. Panaccione, M. Panella, V. Pericoli, D. Ridolfini, L. Pieroni, S. Podda, G.B. Righetti, F. Romanelli, F. Santini, M. Sassi, S.E. Segre, A. Simonetto, C. Sozzi, S. Sternini, O. Tudisco, V. Vitale, G. Vlad, and F. Zonc, Phys. Rev. Lett. **82**, 560 (1999).
[15] D. Pacella, M. May, K.B. Fournier, M. Finkenthal, M. Mattioli, M. Zerbini, M. Leigheb, L. Gabellieri, G. Bracco, F. Crisanti, G. Granucci, M. Marinucci, C. Sozzi, O. Tudisco, G. Giruzzi , P. Buratti, V. Zanza, F. Alladio, B. Angelini, M.L. Apicella, G. Apruzzese, E. Barbato, L. Bertalot, A. Bertocchi, M. Borra, G. Buceti, P. Buratti, A. Cardinali, S. Cascino, C. Centioli, R. Cesario, P. Chuilon, S. Ciattaglia, V. Cocilovo, R. De Angelis, B. Esposito, D. Frigione, L. Gabellierzi, G. Gatti, E. Giovan-

nozzi, M. Grolli, F. Iannone, H. Kroegler, M. Leigheb, G. Maddaluno, G. Mazzitelli, P. Micozzi, P. Orsitto, L. Panaccione, M. Panella, V. Pericoli, L. Pieroni, S. Podda, G.B. Righetti, F. Romanelli, S. Sternini, N. Tartoni, A.A. Tuccillo, V. Vitale, G. Vlad, F. Zonca, A. Bruschi, S. Cirant, S. Nowak, A. Simonetto, V. Mellera, V. Muzzini, F. Gandini, R. Bozzi, and N. Spinicchia (unpublished).

[16] F.H. Seguin, R. Petrasso, and E.S. Marmar, Phys. Rev. Lett. **51**, 455 (1983).

[17] R.A. Hulse, Nucl. Technol./Fusion **3**, 259 (1983).

[18] G. Mazzitelli and M. Mattioli (unpublished).

[19] M. Grolli (unpublished).

[20] B.C. Stratton, H.W. Moos, W.L. Hodge, S. Suckewer, J.C. Hosea, R.A. Hulse, D.Q. Hwang, and J. R Wilson, Nucl. Fusion **24**, 767 (1984).

[21] W.L. Hodge, B.C. Stratton, and H.W. Moos, Rev. Sci. Instrum. **55**, 16 (1984).

[22] Trade Mark of EG&G.

[23] R.J. Fonck, Appl. Opt. **21**, 2115 (1982).

[24] M.A. Graf, Ph.D. thesis, Department of Nuclear Engineering, Massachusetts Institute of Technology, 1995.

[25] D. Pacella, M. Leigheb, and M. Mattioli, Phys. Scr. **57**, 265 (1998).

[26] A.H. Gabriel, Mon. Not. R. Astron. Soc. **160**, 99 (1972).

[27] F. Bely-Dubau, A.H. Gabriel, and S. Volonte, Mon. Not. R. Astron. Soc. **186**, 405 (1979).

[28] R. L. Kelly, J. Phys. Chem. Ref. Data **16** (1987).

[29] D. Pacella, B.C. Gregory, M. Leigheb, G. Pizzicaroli, G. Mazzitelli, M. Borra, L. Pieroni, M. May, K.B. Fournier, W.H. Goldstein, M. Finkentha1, M. Mattioli, F. Alladio, B. Angelini, M.L. Apicella, G. Apruzzese, E. Barbato, S. Belforte, L. Bertalot, A. Bertocchi, G. Bracco, A.Bruschi, G. Buceti, P Buratti, A Cardinali, C. Castaldo, C. Centioli, R. Cesario, P. Chuilon, S.C. Cianfarani, S. Ciattaglia, S. Cirant, V. Cocilovo, F. Crisanti, R. De Angelis, F. De Marco, B. Esposito, D. Frigione, L. Gabellieri, G. Gatti, E. Giovannozzi, C. Gourlan, F. Gravanti, G. Gravanti, G. Granucci, M Grolli, F. Iannone, H Kroegler, G. Maddaluno, G. Maffia, M. Marinucci, P. Micozzi, F. Mirizzi, F.P. Orsitto, L. Panaccione, M. Panella, V. Pericoli-Ridolfini, S. Podda, G.B. Righetti, F. Romanelli, F. Santini, M. Sassi, S.E. Segre, E. Stemini, A. Simonetto, C. Sozzi, N. Tartoni, B. Tilia, A.A. Tuccillo, O. Tudisco, V. Vitale, G. Vlad, V. Zanza, M. Zerbini, and F. Zonca (unpublished).

[30] D. Pacella, B.C. Gregory, L. Gabellieri, G. Mazzitelli, M. Leigheb, G. Pizzicaroli, K.B. Fournier, W.H. Goldstein, M. May, and M. Finkenthal (unpublished).

[31] C. Jordan, Mon. Not. R. Astron. Soc. **142**, 501 (1969).

[32] C. Jordan, Mon. Not. R. Astron. Soc. **48**, 17 (1970).

[33] J.M. Shull and M. Van Steenberg, Astrophys. J., Suppl. Ser. **48**, 95 (1982).

[34] M. Landini and B.C. Monsignori Fossi, Astron. Astrophys., Suppl. Ser. **91**, 183 (1991).

[35] W. Lotz, Astrophys. J., Suppl. Ser. **14**, 207 (1967).

[36] A. Burgess, Astrophys. J. **139**, 766 (1964).

[37] A. Burgess, Astrophys. J. **141**, 1588 (1965).

[38] A. Mertz, R. Cowan, and N. Magee (unpublished).

[39] S.M. Younger, J. Quant. Spectrosc. Radiat. Transf. **27**, 541 (1982).

[40] D. Savin, S. Kahn, J. Linkemann, A. Saghiri, M. Schmitt, M. Grieser, R. Repnow, D. Schwalm, A. Wolf, T. Bartsch, C. Brandau, A. Hoffknecht, A. Muller, S. Schippers, M. Chen, and N. Badnell, Astrophys. J., Suppl. Ser. **123**, 687 (1999).